Glass Physics and Chemistry, Vol. 31, No. 2, 2005, pp. 177–186.

Manganese Ferrite Nanoparticles in Borate Glass and Their Influence on the Magneto-Optical Properties

I. S. Edel'man*, S. A. Stepanov, G. T. Petrovskii**, V. D. Zaikovskii***, R. D. Ivantsov*, O. S. Ivanova*, D. E. Prokof'ev*, T. V. Zarubina**, and E. E. Kornilova****

** Kirensky Institute of Physics, Siberian Division, Russian Academy of Sciences, Akademgorodok, Krasnoyarsk, 660036 Russia*

*** Vavilov State Optical Institute, All-Russia Research Center, ul Babushkina 36/1, St. Petersburg, 192371 Russia*

**** Boreskov Institute of Catalysis, Siberian Division, Russian Academy of Sciences, pr. Akademika Lavrent'eva 5, Novosibirsk, 630090 Russia*

Received August 11, 2004

Abstract—Nanoparticles that are formed in the course of additional heat treatment in borate glasses containing iron and manganese oxide additives at low concentrations are directly observed for the first time using electron microscopy. The size, the shape, and the structure of nanoparticles and their volume distribution in the glass matrix are determined. Correlations between the nanoparticle parameters and the magnetic and magneto-optical properties of the glasses containing these particles are revealed.

INTRODUCTION

Owing to the great diversity of their properties, media containing magnetic nanoparticles have attracted particular attention from researchers and developers of new high-technology materials. The establishment of correlations between the particle characteristics (such as the size, shape, structure, and volume distribution in the sample) and the magnetic and magneto-optical properties is one of the most important problems in the physics and chemistry of nanomaterials. At present, there exist a large number of methods used for synthesizing materials containing magnetic nanoparticles. These methods can be classified according to different factors. In particular, it is expedient to consider two types of nanotechnologies: (1) nanoparticles are formed in an initially homogeneous material during synthesis and subsequent additional treatments, and (2) nanoparticles are synthesized before they are incorporated into a matrix. Glass technologies belong to the former type. Their advantages are the relatively low cost, the possibility of varying the properties of materials over a wide range, the compatibility with the majority of technological materials, and the simplicity of adaptation to the manufacturing of fiber-optic and other optical systems. In 1965, Schinkel and Rathenau [1] were the first to describe oxide glasses that acquire magnetic properties typical of a magnetically ordered material upon introduction of rather large amounts of manganese into the glass composition. Since that time, many researchers have investigated various glasses containing transition-metal oxides [2–6]. As a rule, the magnetic properties have been explained by the precipitation of magnetic microparticles in the glass matrix and observed at a rather high content of paramagnetic oxides (~25–30 wt %). The system of potassium aluminoborate glasses was originally proposed by Skorospelova and Stepanov [7] and was subsequently studied in a number of works [8–10]. The unique feature of this system is that the properties characteristic of magnetically ordered materials manifest themselves at very low contents of paramagnetic additives (~2.0 wt % of the paramagnetic oxide). As a consequence, glasses remain transparent over wide visible and near-IR spectral ranges. This provides prerequisites for their use in the design and preparation of prospective magneto-optical elements. The fundamental approach to the problem of clustering of paramagnetic ions in borate glasses was developed in [8]. However, the extremely high sensitivity of the properties of borate glasses to variations in the conditions of synthesis and additional heat treatments, the multiparameter dependence of the magnetic and magneto-optical properties on these conditions, and the lack of information on the real state of nanoparticles and their distribution in the amorphous matrix have restricted the possibility of optimizing glasses with controlled functional properties. Therefore, an important problem is to establish correlations in the "technological parameters–nanoparticle size and structure–magnetic (magneto-optical) properties" sequence for glasses with a variation in only one technological parameter. According to the data obtained in earlier works [7–10], additional heat treatment is an important stage in the formation of nanoparticles. For this reason, the regime of additional heat treatment was chosen as the varying parameter, whereas the matrix composition $22.5K_2O \cdot 22.5Al_2O_3 \cdot 55B_2O_3$ and the contents (wt %) of paramagnetic oxides $1.5Fe_2O_3$ and 1.5MnO remained unchanged in the experiments. The optical

1087-6596/05/3102-0177 © 2005 Pleiades Publishing, Inc.

Table 1. Heat treatment temperatures of samples and particle diameters (D)

Sample	T_{treat}, °C	D, nm
1	520	–
2	520/6 h	9.0
3	560	25.0
4	600	25.0
5	460 + 600	11.0
6	500 + 560	11.5
7	500 + 600	10.0

absorption and light scattering in glasses of this system were studied in our previous work [11]. It was shown that the optical characteristics of glasses depend drastically on the conditions of additional heat treatment. Moreover, we determined the optimum heat treatment temperatures from the standpoint of the maximum Faraday effect and minimum optical losses. It was assumed that these characteristics are associated with the content and structure of particles in the glass. In this work, we directly observed nanoparticles for the first time.

SAMPLE PREPARATION AND EXPERIMENTAL TECHNIQUE

Glasses were prepared according to a technique similar to that described in [10]. The KNO_3, Al_2O_3, and H_3BO_3 compounds taken in the concentration ratio that provided for the formula corresponding to the K_2O–Al_2O_3–B_2O_3 base glass were used as the initial materials. The Fe_2O_3 and MnO oxides, each at contents of 1.5 wt % over and above 100%, were introduced into the batch. The glasses were melted in platinum crucibles with the use of a platinum agitator at a temperature of 1260°C. Then, the melts were poured onto a steel plate to form 1.0-cm-thick glass plates. The prepared glasses were inertially annealed in a muffle furnace from a temperature of 380°C. Thereafter, the plate was cut into a number of pieces and each piece was subjected to additional heat treatment at different temperatures from 520 to 600°C (Table 1). The heat treatment time at each temperature was equal to 2 h. The sole exception was provided by sample **2**, which was heat treated at a temperature of 520°C for 6 h. This ensured identical compositions and synthesis conditions of the studied samples. The nanoparticle sizes determined using X-ray diffraction analysis in our earlier work [10] are listed in Table 1.

The transmission electron microscope (TEM) images were obtained on a JEM-2010 instrument (resolution, 0.14 nm; accelerating voltage, 200 kV). The phases were identified by electron microdiffraction (EMD) analysis with a locality up to 10 nm. The elemental composition of the samples in different regions was determined using an energy dispersive X-ray analysis (EDXA) (locality, 10–25 nm). For TEM observations, ethanol suspensions of the samples were deposited on perforated carbon substrates fixed on standard copper grids and placed in the chamber of the electron microscope. The field dependences of the magnetization were measured at room temperature on a vibrating-coil magnetometer with a variation in the magnetic field from –12 to + 12 kOe. A nickel film was used as a reference sample for evaluating the magnetization of the glasses. The magnetization was measured accurate to within ±20 Oe. The Faraday effect was measured as a function of the light wavelength in the spectral range 600–2000 nm using the light wave modulation applied to the polarization plane. The accuracy in the measurement of the rotation angle was equal to ±0.2′. The external magnetic field was aligned with the light beam perpendicular to the sample surface and varied from +5 to –5 kOe. The accuracy in the measurement of the field was equal to ±20 Oe.

ELECTRON MICROSCOPIC EXAMINATION

Electron microscopic examination of the samples revealed that the glasses prepared under all heat treatment conditions contain inclusions of $MnFe_2O_4$ particles whose morphological parameters (shape, size, character of aggregation) depend on the heat treatment regime. Therefore, we confirmed the assumption that nanoparticles are also formed in the X-ray amorphous samples (sample **1**). The TEM micrographs, the electron diffraction patterns, and the EDXA spectra are depicted in Figs. 1–4. The characteristics of nanoparticles in the samples are presented in Table 2. It can be seen from Fig. 1c that the micrograph of sample **3** heat treated at 560°C differs substantially from the other micrographs. The heat treatment at temperatures lower than 560°C leads to the formation of oval small-sized disordered particles (~4–6 nm) united into aggregates with linear sizes of ~20 nm (Fig. 1a). An increase in the time of heat treatment at the same temperature results in an increase in the size of particles inside aggregates (to ~10 nm), the growth of aggregates (to ~25 nm), and the appearance of faceting (Fig. 1b). In both cases, the aggregate sizes are close to each other and somewhat smaller than the size of well-faceted particles in sample **3** (Fig. 1c). We can assume that, at a temperature of 560°C, the ionic mobility provides the formation of particles together with their sintering and ordering. Upon heat treatment at higher temperatures, small-sized particles crystallize earlier (Fig. 1d) than they unite into larger sized particles. In this case, the most important parameter is the temperature at the first heat treatment stage, because heat treatment at a higher temperature at the second stage (samples **5**–**7**) does not lead to the formation of large-sized crystals with good faceting. At the same time, the mean distances between

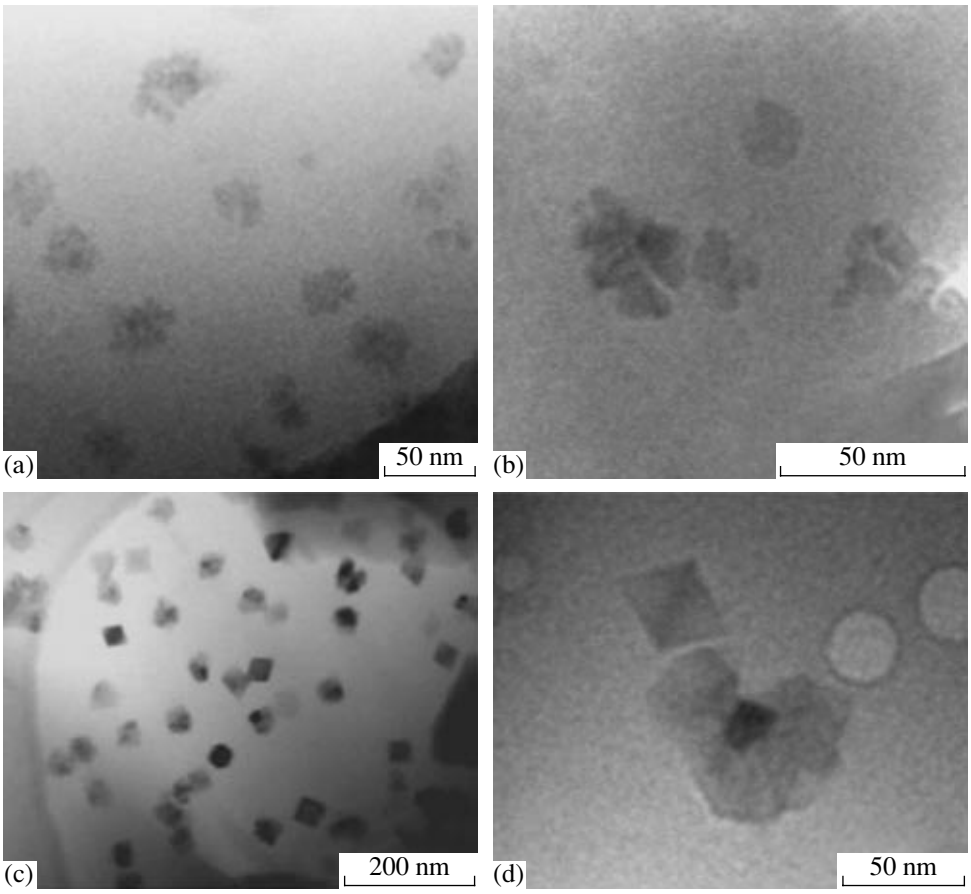

Fig. 1. TEM micrographs of fragments of samples (a) **1**, (b) **2**, (c) **3**, and (d) **4**.

large-sized particles or aggregates composed of small-sized particles are approximately identical for all the samples (~50 nm). The analysis of the electron diffraction patterns demonstrates that the structure of particles corresponds to the structure of the $MnFe_2O_4$ manganese ferrite. This is in agreement with the X-ray diffraction data obtained earlier in [10]. The electron diffraction patterns of some samples are shown in Fig. 2.

The EDXA spectra measured for different regions of the glass samples with and without nanoparticles allow us to determine the ratio between the paramagnetic elements in these regions. As an example, Fig. 3 shows the EDXA spectra obtained for different regions of sample **3**. The $n_{Fe} : n_{Mn}$ elemental ratio determined for an isolated crystalline inclusion in the glass is in reasonable agreement with the ratio of these elements in a $MnFe_2O_4$ crystal. However, the EDXA spectrum of the region free from crystalline particles (according to the TEM data) indicates the presence of Fe and Mn (in trace amounts).

The EDXA spectrum of the region free from crystalline particles in sample **1** (Fig. 4) demonstrates that this region contains the above elements in considerable amounts. These elements either enter into the composition of finely dispersed particles (unobservable under the electron microscope) or are incorporated into the glass in the ionic form. Most likely, the content of finely dispersed inclusions decreases with an increase in the temperature of heat treatment of the samples due to the partial sintering of the components introduced into the glass. This can be judged from the comparison of Figs. 3a and 4.

The analysis of the X-ray diffraction data (Table 1) and the TEM data permits us to make the inference that even the X-ray amorphous glass samples involve crystalline nanoparticles. The shape, size, and structure of particles and their volume distribution in the matrix, as well as the content of elements in glass regions free from particles, depend on the heat treatment temperature. The manganese and (or) iron oxide phases can be observed in the vicinity of the ferrite phase. The size and volume distributions of particles in the matrix are most uniform in the samples heat treated at 560°C.

MAGNETIC MEASUREMENTS

The field dependences of the magnetization $M(H)$ for two typical samples are plotted in Fig. 5. The coin-

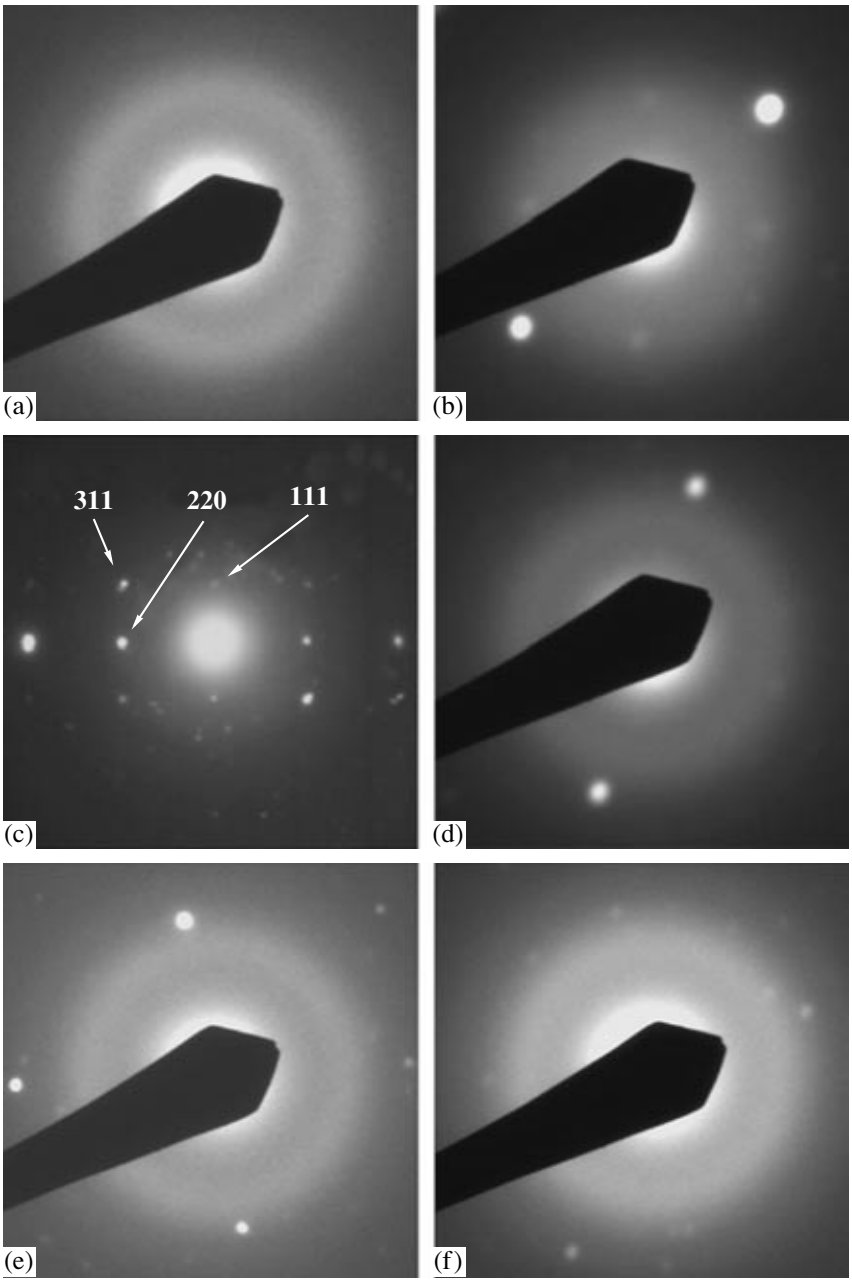

Fig. 2. Electron diffraction patterns of individual particles in samples (a) **1**, (b) **2**, (c) **3**, (d) **4**, (e) **5**, and (f) **6**.

cidence of the curves $M(H)$ for two orientations of the external magnetic field, namely, the orientations parallel and perpendicular to the plane of the glass plates, suggests that the macroscopic magnetic anisotropy is absent in the samples. The high magnetic susceptibility in low fields, the magnetic saturation, and the magnetic hysteresis confirm that the glass contains a ferromagnetic or ferrimagnetic phase. The magnetizations normalized to the sample mass are given in Table 3. Rather large sizes of particles in sample **3** and their uniform volume distribution in the glass enable us to estimate the saturation magnetization of the particle material. The saturation magnetization turns out to be approximately equal to 50 G cm^3 g^{-1}; i.e., it is rather close to the known magnetization of the manganese ferrite (80 G cm^3 g^{-1}) at room temperature [12]. Moreover, it can be seen from Fig. 5 and Table 3 that the magnetization in the maximum field and the behavior of the magnetization curve depend on the particle size. The magnetization measured for the samples in a field of 10 kOe decreases in the order **3 > 4 > 7 > 6 > 2 > 5 > 1**. It was found that, at the same initial content of paramagnetic

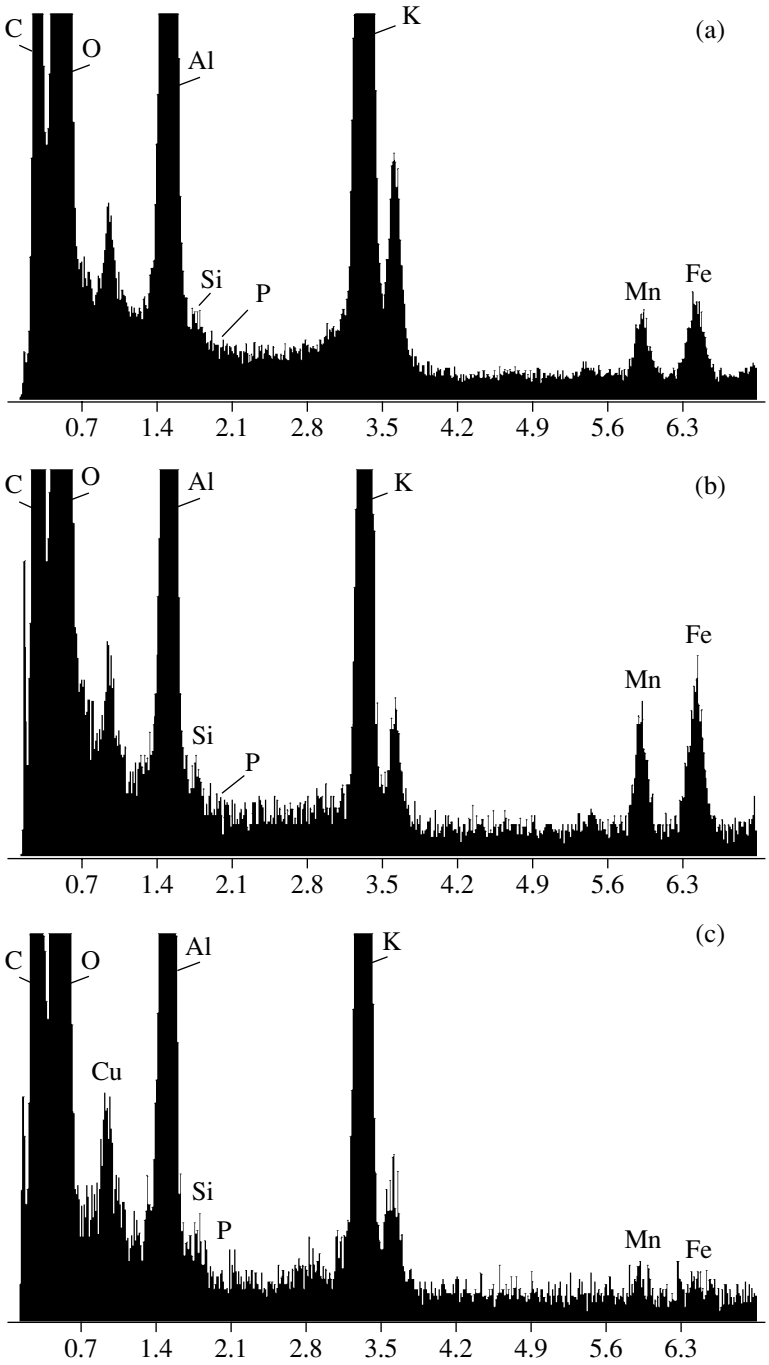

Fig. 3. EDXA spectra of three regions in sample **3**: (a) the large-sized region including several particles, (b) one particle, and (c) the region free from particles.

components in the glass, the maximum and minimum magnetizations measured in a field of 10 kOe differ by a factor of more than two. This can be partially explained by the increase in the fraction of paramagnetic ions that enter into the composition of particles at optimum temperatures of heat treatment. However, a comparison of Figs. 2 and 3 demonstrates that this cannot be the main factor explaining so strong a difference between the magnetizations of the samples and also between their magnetization and the magnetization of a massive manganese ferrite. This difference can be associated with the incorporation of diluting ions of the matrix (most probably, Al^{3+} ions) into the ferrite phase, the deviation of the ferrite composition from stoichiometry, the increase in the degree of inversion of the ferrite, and the change in the valence of paramagnetic

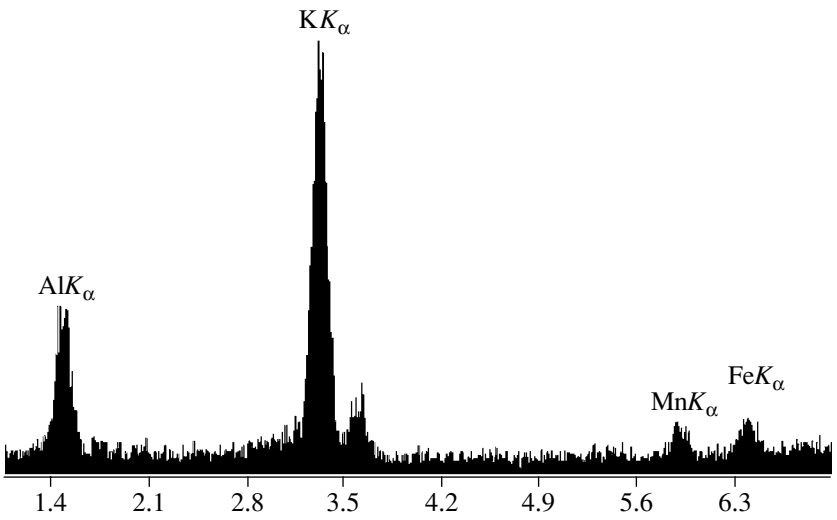

Fig. 4. EDXA spectrum of the region free from particles in sample **1**.

ions. The effect of the aforementioned factors virtually does not depend on the measurement temperature. We can argue with a high probability that their contribution should decrease when the particle structure becomes similar to the structure of a manganese ferrite single crystal. The magnetization of nanoparticles and its field dependences should be strongly affected by the size effects whose contribution depends on the measurement temperature. First and foremost, this is the transition from a superparamagnetic state to a blocked state. Such a transition, as applied to glasses in the system under investigation, was considered in our previous work [9]. A comparison of the magnetization curves depicted in Fig. 5 with the data obtained in [9] suggests that the main contribution to the magnetization of samples **1**–**7** at room temperature is determined by the blocked particles, which are responsible for the remanent magnetization. (The last inference will be more clearly evidenced by the field dependences of the Faraday effect.) However, particles 2–5 nm in size at room temperature should undergo a magnetization reversal of the superparamagnetic type. Their transformation into the blocked state with a decrease in the temperature should result in an increase in the magnetization of the sample. The contribution of ions located in surface layers of particles also depends on the measurement temperature. A considerable imperfection of the particle structure on the surface and, more importantly, a change in the coordination of paramagnetic ions and disturbance of interionic exchange coupling in the surface layer result in the formation of a spin-glass state [13]. The "freezing" of this state with a decrease in the

Table 2. Characteristics of nanoparticles distributed in the glass samples

Sample	Structural and morphological parameters of $MnFe_2O_4$ particles according to transmission electron microscopy and electron microdiffraction
1	Loose microaggregates 30–40 nm in size (Fig. 1a) consist of small-sized particles (2–5 nm). There are isolated small-sized particles. The electron diffraction pattern is typical of an amorphous state (Fig. 2a).
2	Microaggregates 30–40 nm in size (Fig. 1b) are composed of small-sized particles (2–10 nm). There are isolated small-sized particles. The electron diffraction pattern is characteristic of a polycrystal and contains a large number of reflections (Fig. 2b).
3	Isolated particles 40–50 nm in size have a cubic morphology (Fig. 1c). The electron diffraction pattern corresponds to a manganese ferrite single crystal (Fig. 2c).
4	Crystals 30–50 nm in size (Fig. 1d) frequently form aggregates consisting of several crystals. There is a very small number of aggregated finely dispersed particles (2–5 nm). The electron diffraction pattern corresponds to a point single crystal (Fig. 2d).
5	Crystals 30–50 nm in size frequently form aggregates composed of several crystals. There are aggregates of particles 2–10 nm in size. The electron diffraction pattern is characteristic of a polycrystal and contains a large number of reflections (Fig. 2e).
6 and **7**	Analogs of sample **5**

temperature also leads to an increase in the magnetization. The separation of these two mechanisms is a very complex problem, because the contributions of both mechanisms to the magnetization identically depend on the particle size; specifically, they increase with a decrease in the particle size. Moreover, the temperature dependence of the magnetization should be analyzed with allowance made for the known increase in the magnetization of the manganese ferrite with a decrease in the temperature [12]. However, the temperature dependences of the magnetization permit us to reveal qualitatively the mechanism that makes a larger contribution to the difference between the magnetizations of an ensemble of particles in the glass and the massive ferrite. Such an estimate will be made from the data on the Faraday effect.

FARADAY EFFECT

A comparative analysis of the spectral dependences of the Faraday effect for the studied glasses and a massive manganese ferrite single crystal $MnFe_2O_4$ in our earlier work [10] demonstrated their close agreement. In the present work, we examine the field dependences of the Faraday effect and compare the magnitudes of the Faraday effect and its temperature dependences for different types of particles that are formed in the samples heat treated under different conditions. Figure 6 shows the hysteresis loops determined by measuring the Faraday effect, which is more sensitive in the range of low magnetic fields. The hysteresis loop of sample **3** has a shape that is most similar to rectangular with the remanent magnetization equal to half the saturation magnetization M_s. For sample **1** containing only small-sized amorphous particles, the relative magnitude of the remanent Faraday effect is considerably smaller and the gradient of the Faraday effect with respect to the field in high fields is larger than those for the other samples. In this case, the remanent Faraday effect indicates that a number of particles at room temperature are in the blocked state. Since the linear sizes of these particles are equal to 2–5 nm, we can make the inference that a size of ~5 nm corresponds to the transition between the superparamagnetic and blocked states of particles at room temperature. The field dependences of the Faraday effect for other samples are intermediate between the aforementioned two dependences. The relatively high magnetic susceptibility in high fields is associated with the smaller sized particles, whereas the considerable remanent magnetization is due to the large-sized particles. It remains unclear whether particles interact with each other in aggregates and how this interaction affects the field dependences of the magnetization and the Faraday effect. Unlike the magnetization, the maximum Faraday effect is observed for two samples, **3** and **4**, whereas the maximum remanent Faraday effect occurs in sample **3**. Therefore, the heat treatment at 560°C is optimum for providing a substantial Faraday effect in relatively low magnetic fields and a consider-

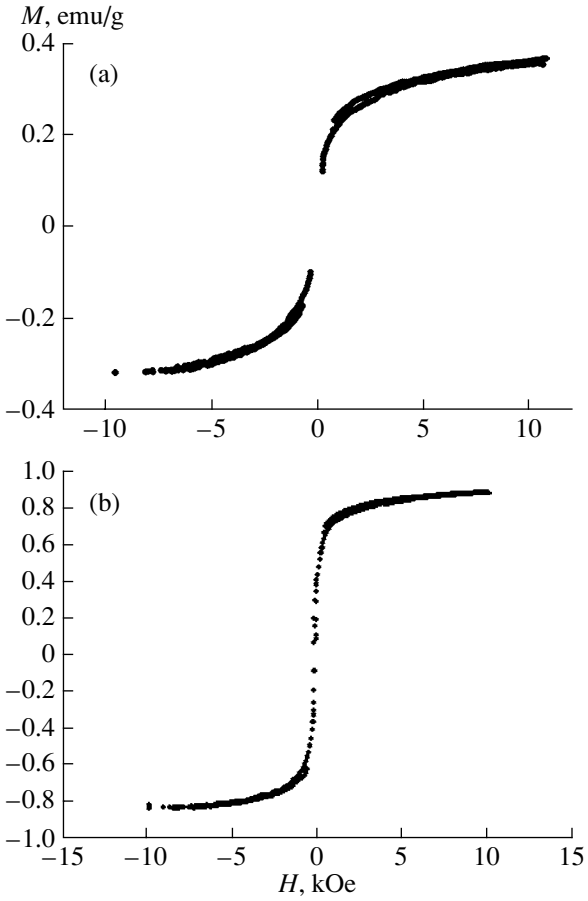

Fig. 5. Magnetization curves measured on a vibrating-coil magnetometer for samples (a) **1** and (b) **3**.

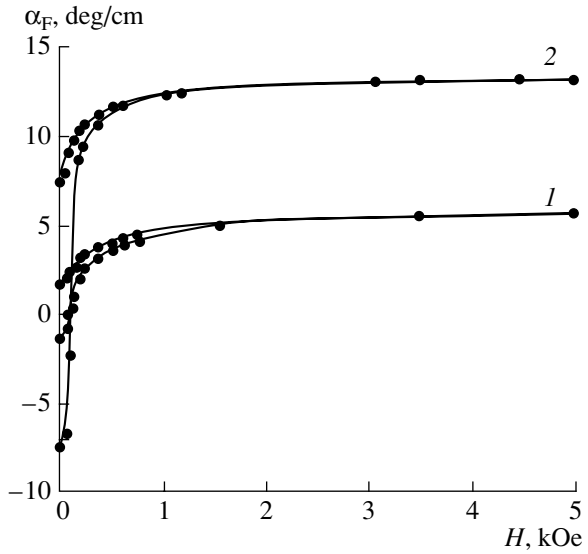

Fig. 6. Field dependences of the Faraday effect for samples (*1*) **1** and (*2*) **3**.

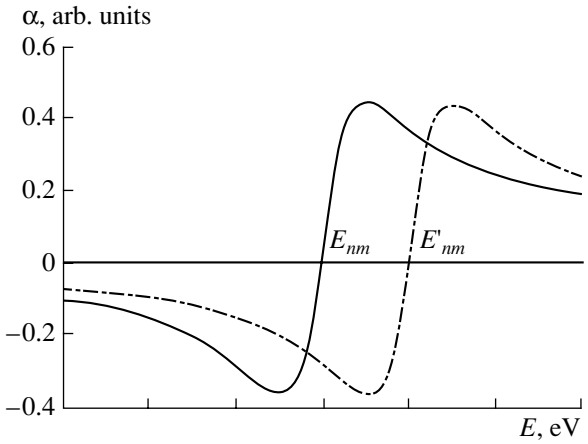

Fig. 7. Schematic illustration of the dispersion of the Faraday effect for two different transition energies E_{nm}.

able remanent Faraday effect. A comparison with the TEM data allows us to make the unique inference that the magnetic and magneto-optical properties of glasses are optimum when the most perfect crystalline particles, which are almost uniformly distributed in the matrix and are not prone to aggregation (as compared to particles in the samples heat treated under other conditions), are formed in the glass.

The ratios between the magnitude of the Faraday effect measured in the field $H = 2.0$ kOe and the magnetization in the same field are presented in Table 3. It is worth noting that the ratio α/M varies from sample to sample. One of the possible reasons for this variation can be the redistribution of Fe^{3+} and Mn^{2+} cations between the tetrahedral and octahedral sublattices with a variation in the structure and size of particles. Since the magnetic moments of these ions are equal to each other, their migration from one crystallographic position to another position is not accompanied by a change in the total magnetic moment of the sample. Unlike magnetization, the Faraday effect is determined not only by the difference between the numbers of ions in two magnetic sublattices with opposite spin orientations but also depends on the energy and oscillator strengths of electron transitions, which determine the spectral dependence of the Faraday effect. As is known, the Faraday effect associated with the paramagnetic ions is described by the relationship

$$\alpha \approx \frac{2\pi\frac{e^2}{m}\Delta N_{nm}(E_{nm}^2 - E^2)}{(E_{nm}^2 - E^2)^2 + E^2\gamma^2}, \quad (1)$$

where e is the electron charge, m is the electron mass, E_{nm} is the energy of the electron transition between the levels m and n, ΔN_{nm} is the difference between the numbers of atoms residing in the states m and n, and γ is the line width. Relationship (1) for two different energies E_{nm} is schematically illustrated in Fig. 7. It can be seen that that the larger the energy separation from the transition energy E_{nm} in the spectrum, the smaller the magnitude of the Faraday effect. In turn, the transition energy E_{nm} is governed by the crystal field energy, which is different for tetrahedral and octahedral positions [14]. The migration of a particular cation, for example, a Fe^{3+} cation, from one position to another position leads to a change in the energy of the electron transition and its oscillator strength. The shift of the electron transition to the high-energy range results in a weakening of the Faraday effect in the infrared range, as can be seen from Fig. 7. Such a mechanism requires the assumption that cations are redistributed between the sublattices with a variation in the structure, shape, and size of particles. At present, in order to provide a deeper insight into this problem, we have investigated the distribution of cations over the sublattices.

The change in the magnitude of the Faraday effect with a decrease in the temperature is illustrated by the data presented in Table 4. A decrease in the measurement temperature in the range 300–105 K results in an increase in the magnitude α_{max} of the Faraday effect for all the samples and in the ratio α_0/α_{max} for the majority of the samples. In the aforementioned temperature range, the magnitude α_{max} of the Faraday effect increases almost linearly with a decrease in the temper-

Table 3. Magnetization M of samples at two external magnetic field strengths of 10 and 2 kOe, the magnitude α of the Faraday effect at a magnetic field strength of 2 kOe, and ratios of the magnitude of the Faraday effect to the magnetization

Sample	$M_{H=10\text{ kOe}}$, G cm^3 g^{-1}	$M_{H=2\text{ kOe}}$, G cm^3 g^{-1}	$\alpha_{H=2\text{ kOe}}$, deg/cm^{-1} (800 nm)	α/M at $H = 2$ kOe
1	0.36	0.27	5.03	18.63
2	0.48	0.39	6.7	17.18
3	0.89	0.80	18.56	23.2
4	0.66	0.57	18.50	32.46
5	0.46	0.36	10.48	29.11
6	0.49	0.39	7.35	18.45
7	0.54	0.40	7.83	19.58

Table 4. Magnitudes of the Faraday effect at λ = 935 nm in zero and maximum (3.5 kOe) magnetic fields (α_0 and α_{max}, respectively), ratios α_0/α_{max} at two temperatures, temperature coefficients $C_T = [(\alpha_{105\ K} - \alpha_{300\ K})/\alpha_{300\ K}] \times 100\%$, and magnitudes of the Faraday effect measured in a magnetic field of 0.2 kOe at a wavelength of 1.5 μm

Sample	α_0(300 K), deg/cm	α_0(105 K), deg/cm	α_{max}(300 K), deg/cm	α_{max}(105 K), deg/cm	α_0/α_{max} (300 K)	α_0/α_{max} (105 K)	C_T	α (λ = 1.5 μm, H = 0.2 kOe), deg/cm
1	0.27	1.8	2.96	6.95	0.09	0.26	1.35	1.0
2	1.07	4.12	6.73	14.23	0.16	0.3	1.15	1.6
3	10.32	15.28	21.77	35.34	0.47	0.43	0.63	4.2
4	8.4	12.72	18.84	31.1	0.45	0.41	0.65	3.7
5	2.08	6	11.82	20.03	0.18	0.3	0.69	2.1
6	1.03	4.36	8.09	15.44	0.13	0.28	0.91	1.6
7	0.91	4.87	9.18	16.81	0.1	0.3	0.83	1.5

ature. The rate of increase in the magnitude α_{max} of the Faraday effect can be defined as the temperature coefficient $C_T = (\alpha_{105} - \alpha_{300})/\alpha_{300}$, which differs for different samples (Table 4). The largest temperature coefficient C_T is observed for sample **1** containing particles with the smallest sizes. The increase in the ratio α_0/α_{max} with a decrease in the temperature is also largest for this sample. Therefore, the larger the particle size, the larger the magnitude α_{max} of the Faraday effect, whereas the smaller the particle size, the larger the temperature coefficient C_T. An increase in the magnitude of the Faraday effect upon cooling of the samples considerably exceeds an increase in the magnetization of the manganese ferrite upon cooling in the corresponding temperature range [12]. According to the data presented in Table 4, the magnetization of the manganese ferrite increases by 36% with a decrease in the temperature range 300–105 K. Consequently, as the temperature decreases, the smaller the particle size, the larger the increase in the magnetization of the glasses as compared to the magnetization of the massive manganese ferrite. This fact indicates that size effects substantially contribute to the magnetic properties of the studied glasses.

The magnitudes of the Faraday effect at a wavelength of 1.5 μm (Table 4) suggest that samples **3** and **4** have a high magneto-optical quality.

CONCLUSIONS

Thus, it has been shown that the magnetic, optical, and magneto-optical properties of borate glasses containing iron and manganese additives at low contents are associated with the formation of manganese ferrite particles. The size, the shape, and the structure of nanoparticles and their distribution in the glass matrix at identical contents of paramagnetic additives are determined by the conditions of additional heat treatments. Nanoparticles with parameters closest to those of a manganese ferrite single crystal are formed upon heat treatment of glasses at a temperature of 560°C. Samples containing these nanoparticles have optimum parameters from the standpoint of practical applications: the magnitude of the Faraday effect, the magnetization, the remanent Faraday effect, and the magnetic susceptibility in weak magnetic fields are maximum for these samples. The conclusion was drawn that the unusual temperature behavior of the Faraday effect and the temperature dependence of the ratio α/M are most likely due to the size effects in nanoparticles.

REFERENCES

1. Schinkel, C.J. and Rathenau, G.W., Magnetic Interactions in Borate Glasses Containing Manganese Ions, in *The Physics of Non-Crystalline Solids*, Amsterdam: North-Holland, 1965, pp. 215–219.
2. Tsang, C., Gafney, H.D., Sunil, D., Rafailovich, M., Sokolov, J., and Gambino, R.J., High Coercivity Single-Domain Particles in Glass Matrix, *J. Appl. Phys.*, 1996, vol. 79, pp. 6025–6027.
3. Berger, R., Kliava, J., Bissey, J.-C., and Baïetto, V., Magnetic Resonance of Superparamagnetic Iron-Containing Nanoparticles in Annealed Glasses, *J. Appl. Phys.*, 2000, vol. 87, pp. 7389–7396.
4. Li, L.P., Li, G.S., and Smith, R.L., Microstructural Evolution and Magnetic Properties of $NiFe_2O_4$ Nanocrystals Dispersed in Amorphous Silica, *Chem. Mater.*, 2000, vol. 12, pp. 3705–3714.
5. Rajic, N., Ceh, M., and Gabrovsek, R., Formation of Nanocrystalline Transition-Metal Ferrites Inside a Silica Matrix, *J. Am. Ceram. Soc.*, 2002, vol. 5, pp. 1719–1724.
6. Ponce-Castaneda, S., Martinez, J.R., Palomares Sanchez, S.A., Ruiz, F., Ayala-Valenzuela, O., and Matutes-Aquino, J.A., Formation of Nickel–Zinc Ferrite Embedded in a Silica Xerogel Matrix, *J. Sol–Gel. Sci. Technol.*, 2002, vol. 25, pp. 37–41.
7. Skorospelova, V.I. and Stepanov, S.A., Behavior of Iron Ions in Glasses of the K_2O–Al_2O_3–B_2O_3 System, *Izv. Akad. Nauk SSSR, Neorg. Mater.*, 1974, vol. 10, pp. 1864–1871.

8. Stepanov, S.A., Clusters of Paramagnetic Ions in Glasses, *Fiz. Khim. Stekla*, 1976, vol. 2, no. 3, pp. 228–233.
9. Edelman, I., Ivantsov, R., Vasiliev, A., Stepanov, S., Kornilova, E., and Zarubina, T., *Physica B* (Amsterdam), 2001, vol. 301, pp. 203–211.
10. Edelman, I., Ivantsov, R., Vasiliev, A., Stepanov, S., Kornilova, E., and Zarubina, T., Magnetic Properties of Nano-Crystalline Ferrite Particles in Alumina–Borate Glass Matrix, *Phys. Met. Metallogr.*, 2001, vol. 91, Suppl. 1, pp. 116–120.
11. Stepanov, S.A., Petrovskii, G.T., Zarubina, T.V., Kornilova, E.E., and Edel'man, I.S., Spectral Properties of Magneto-Optical Glasses Containing Manganese Ferrite Nanoparticles, *Opt. Zh.*, 2003, vol. 70, pp. 46–53.
12. Smit, J. and Wijn, H.P.J., *Ferrites*, Eindhoven: Philips Technical Library, 1959.
13. Kodama, R.H., Magnetic Nanoparticles, *J. Magn. Magn. Mater.*, 1999, vol. 200, pp. 3590–3596.
14. Kucera, M., Kolobanov, V.N., Mikhailin, V.V., Orekhanov, P.A., and Makhov, V.N., Reflection Spectra of Some Garnet and Orthoferrite Single Crystals in Vacuum Ultraviolet, *Phys. Status Solidi B*, 1990, vol. 157, pp. 745–752.